Partial melting mechanisms of embedded nanocrystals

J. A. Pakarinen, M. Backman, F. Djurabekova, and K. Nordlund*
Department of Physics and Helsinki Institute of Physics, University of Helsinki, P.O. Box 43, FIN-00014 Helsinki, Finland
(Received 31 December 2008; published 24 February 2009)

Understanding the melting mechanisms of nanocrystals embedded in solids is of great current interest since both the synthesis and modification of such systems frequently involve the use of high temperatures. Using molecular-dynamics computer simulations we study the melting mechanisms of Cu, Ag, and Au nanoclusters embedded in metal matrices and Si nanocrystals in amorphous silica. The results show that nanocrystals embedded in a solid bulk material with a higher melting temperature exhibit complex melting behavior and can even, in the same system, exhibit four distinct stages prior to full melting of the system.

DOI: 10.1103/PhysRevB.79.085426 PACS number(s): 61.46.Hk, 65.80.+n, 02.70.Ns, 82.60.Qr

I. INTRODUCTION

The thermodynamic properties of nanoclusters in vacuum and dilute gases have been studied extensively.[1] They have been found to exhibit interesting behavior with no counterpart in conventional thermodynamics, such as temperature regions where a cluster may fluctuate between ordered and disordered regions, thus making the melting temperature ill defined.[1] On the other hand, the thermodynamic properties of nanoclusters embedded inside solids have been studied much less than those of clusters in vacuum, in spite of their great potential for practical application in optoelectronics and memory circuits.[2,3]

While nanoclusters in vacuum are well known to usually melt at temperatures much below the normal bulk melting point[1,4] (with the exception of some very small systems with only a few tens of atoms[5,6]), embedded nanoclusters have been variously reported to melt below or above the bulk melting temperature.[4,7–20] Perhaps the most intriguing is the experimental[4] and computational evidence[21] of embedded or coated nanoclusters which shows that even in the same system, the melting point can be either lowered or increased depending on the nature of the interface. Several different theoretical models have been proposed to explain the melting mechanisms in embedded nanoclusters but it is not clear which, if any, of them has general validity (for a recent review see Ref. 4, and references therein).

In the current work we employ molecular-dynamics (MD) computer simulations to study the atom-level melting mechanism of nanocrystals embedded in solids, with the aim to determine how many stages precede full melting of an embedded nanocluster system. We focus the study on face-centered-cubic (fcc) metal nanocrystals inside other fcc metals but also examine Si nanocrystals in amorphous silica to show that the results have validity also in a quite different kind of system.

II. METHOD

We examine the melting mechanisms of embedded nanocrystals using MD simulations—the same approach that have given much valuable insight into the thermodynamics of nanoclusters in vacuum (see, e.g., Refs. 6 and 22–26). We chose to study metal nanocrystals inside fcc metals since this system is well known with respect to other properties[27,28] and well-tested potentials exist for them,[28,29] as well as Si nanocrystals inside amorphous silica due to their great application potential.[2,30,31] The specific metal combinations chosen were Cu nanoclusters in Co matrices and Ag and Au nanoclusters in Cu matrices. We focused in particular on the case of Cu in Co since these metals have a large melting point difference. The MD simulations were carried out using the PARCAS code—well tested in simulation of nanoclusters.[25,32–34] For the metals we used embedded-atom method type of potentials[35,36] and for the Si-silica system we used an angular- and environment-dependent potential known to describe well the structure of both pure Si and amorphous silica.[37,38]

The nanocrystals were cut out as spheres from the equilibrium bulk crystal structures, with diameters in the range of 0.8–6 nm. They were then inserted into the surrounding matrix material, into a spherical hole cut into exactly the same size, after rotation at a random angle in the center of the simulation cell. Periodic boundary conditions were used in all dimensions. The lattice constant for the cluster and matrix was that of each element in equilibrium in the bulk phase at each temperature. The metal matrices were created directly in the fcc crystal structure, while amorphous silica was prepared as described in Refs. 39 and 40. Prior to insertion, the cluster was slightly compressed so that no pair of atoms would initially be unrealistically close to each other. The system was then simulated for 5 ps at 100 K so that the cluster obtained a realistic interface with the surroundings. The surrounding system was a cube two times larger than the cluster diameter in all dimensions (a few cases were repeated with three times larger cubes and showed identical melting behavior). For each combination of elements, cluster size, and temperature, 5–16 simulations with random initial rotation were carried out to obtain statistics.

After the creation of the embedded nanocrystal, the actual melting simulations were carried out. The system was raised up to the desired temperature over 50 ps, after which it was simulated at least for 100 ps at each temperature T. The temperature control of Berendsen *et al.*[41] was used for heating and for keeping the cell at the desired temperature. The time constant was set to 5 ps, which is sufficiently large to allow natural temperature fluctuations in the system. The pressure control of Berendsen *et al.*[41] with a time constant of 1 ps was used to keep the cell at zero pressure.

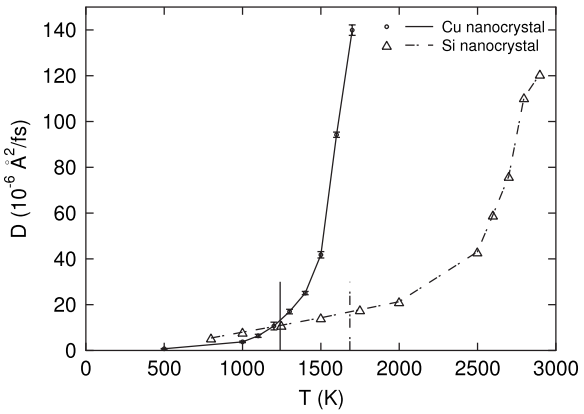

FIG. 1. Diffusion constant of the nanocrystal atoms only for Cu nanocrystals in Co and Si nanocrystals in silica. The short vertical lines show the melting points of the nanocrystal elements in the bulk phase within the potential model used.

The behavior of the system was analyzed by visual inspection of cross sections of the simulation cell, by determining the diffusion constant D from the mean-square atom displacements divided by simulation time, and by using angular structure factor analysis (see Sec. III C). D was determined separately for the cluster atoms only (after the final temperature had been reached), as well as the whole simulation cell. Since atoms can move by each other in a liquid, melting is clearly visible as a sharp increase in $D(T)$ with increasing temperature.

III. RESULTS

Since we obtained the most comprehensive set of results for the system of Cu nanoclusters in Co, we will focus the discussion on this system, and we will mention explicitly if the results are for one of the other systems. As a function of cluster size, the initial structure of the clusters behaved overall as follows. Cu clusters smaller than 2 nm become, already in the initial relaxation stage, epitaxial with the surrounding matrix regardless of their initial rotation. Clusters in the size range 2–3 nm generally became epitaxial with the matrix either in the relaxation or initial stage of the long simulations but some defects remained in them (since the lattice constants do not match, a perfect match of atom numbers for epitaxiality is unlikely). Clusters that are 4 nm or larger in size kept their random orientation.

A. Diffusion

The behavior of the diffusion constant as a function of temperature is illustrated in Fig. 1. As expected, at the highest temperatures, $D(T)$ rises rapidly as the system melts and the atoms become highly mobile in the molten phase. However, the behavior prior to the sharp rise is interesting. Instead of a diffusion constant of almost exactly zero which would be expected in a perfect crystal (note that diffusion by thermally generated vacancies is not possible here since no vacancy source is present in the simulated system), $D(T)$ clearly differs from zero before the sharp rise (T range from 1050 to 1450 K for Cu and 1000 to 2500 K for Si). While the shape is qualitatively the same in both cases, the curves are shifted with respect to each other because of the difference in melting point in the materials in the bulk phase. This indicates that premelting behavior allows for enhanced atom motion prior to the melting of the whole system.

B. Mechanisms

Careful visual analysis of the system as well as quantitative angular structure factor analysis revealed that in fact at least four different mechanisms are active below the melting temperature of the whole system $T_{\mathrm{melt,system}}$. These are numbered (i)–(iv) and described as follows. The mechanisms are illustrated in Figs. 2 and 3 and in the animations available in the supplementary EPAPS material.[42]

(i) As mentioned above, some of the clusters contain defects. These become mobile at some temperature and tend to migrate to the interface, where they remain in motion. The defect migration increases the diffusion constant. Since the defects tend to remain at the interface, this mechanism can also be considered partial interface melting. In the smallest (<2 nm) systems, which became epitaxial and contained no defects, some atom exchange was observed, which is likely made possible due to the large strain in the system.

(ii) At slightly higher temperatures, the clusters were observed to fluctuate between different states. They could, e.g., switch back and forth between an epitaxial and random state, and ordered and disordered structures. This stage is different from stage (i) such that the fluctuations occur everywhere in the cluster and not only at the interface. The lowest temperature at which either mechanism (i) or (ii) became active is defined as the partial melting temperature $T_{\mathrm{melt,partial}}$.

(iii) At some temperature, the nanocrystal melted completely. This temperature is defined as the nanocluster melting temperature $T_{\mathrm{melt,cluster}}$ and is the one where $D(T)$ starts its rapid rise.

(iv) Above $T_{\mathrm{melt,cluster}}$ but below the melting temperature of the matrix, the strain associated with the cluster may destabilize the surrounding cluster matrix, leading to a "melting" (formation of a disordered zone with decreased order parameter[43]) of also the matrix material at the interface with the nanocluster.

The snapshots on the melting mechanisms in Fig. 2 and animations are, for clarity, made on atom positions averaged over time to reduce the effects of thermal vibrations around the equilibrium position. To provide a point of comparison, Fig. 3 shows atom positions which are not averaged over time. In the 0 ps snapshots, the atoms look well ordered since the cell is at 100 K, but for the snapshots at larger times the large thermal fluctuations in Fig. 3 make interpretation of the results more difficult. However, fluctuations between states [mechanism (ii)] and melting of the bulk part of the interface [mechanism (iv)] are also fairly well visible in the non-time-averaged plot (Fig. 3).

Diffusion constant and visual analysis was carried out to determine which mechanisms are present for all simulated cluster size and temperature combinations in the Cu in Co system. The results are illustrated as a phase-diagram-like

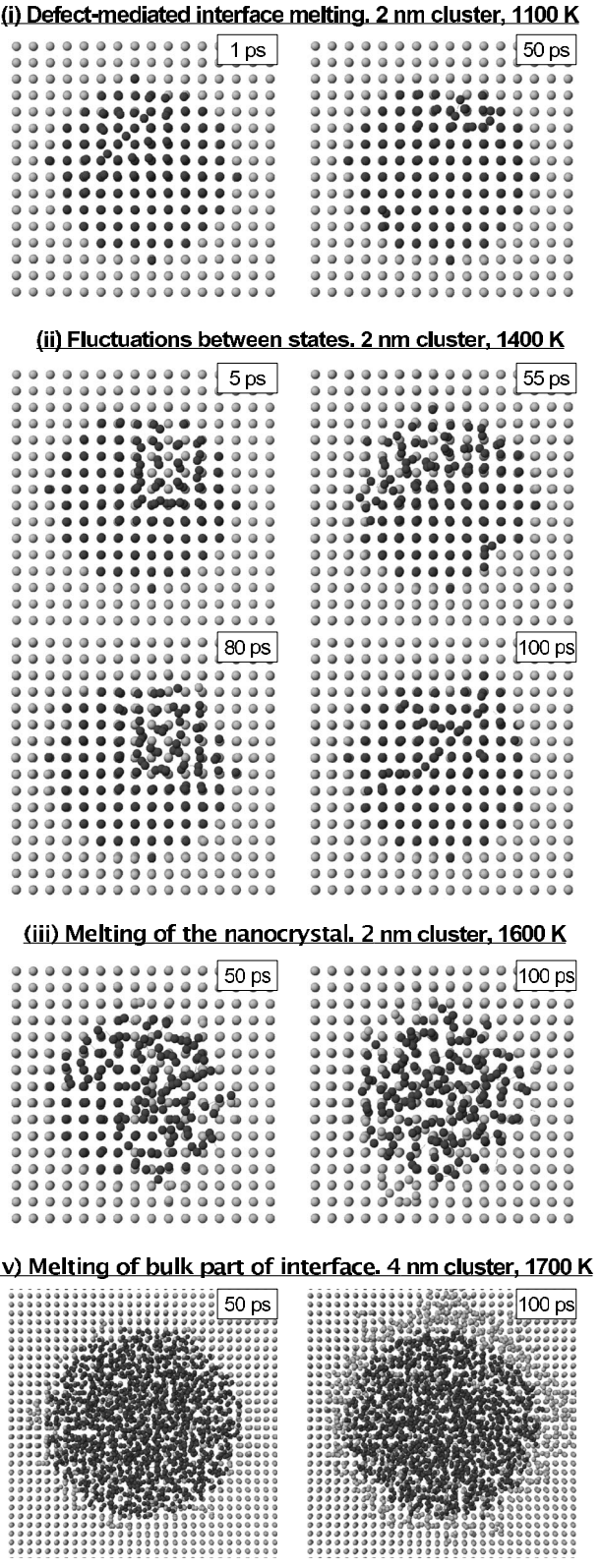

FIG. 2. Illustration of the melting mechanisms of Cu nanocrystals in Co. The atom positions are time averaged over intervals of a few picosecond. Darker spheres illustrate Cu atoms and lighter ones illustrate Co. The figures are cross sections of the middle of the simulation cells. The temperatures indicate the final temperature in the system, to which the temperature is raised over the first 50 ps in the simulations.

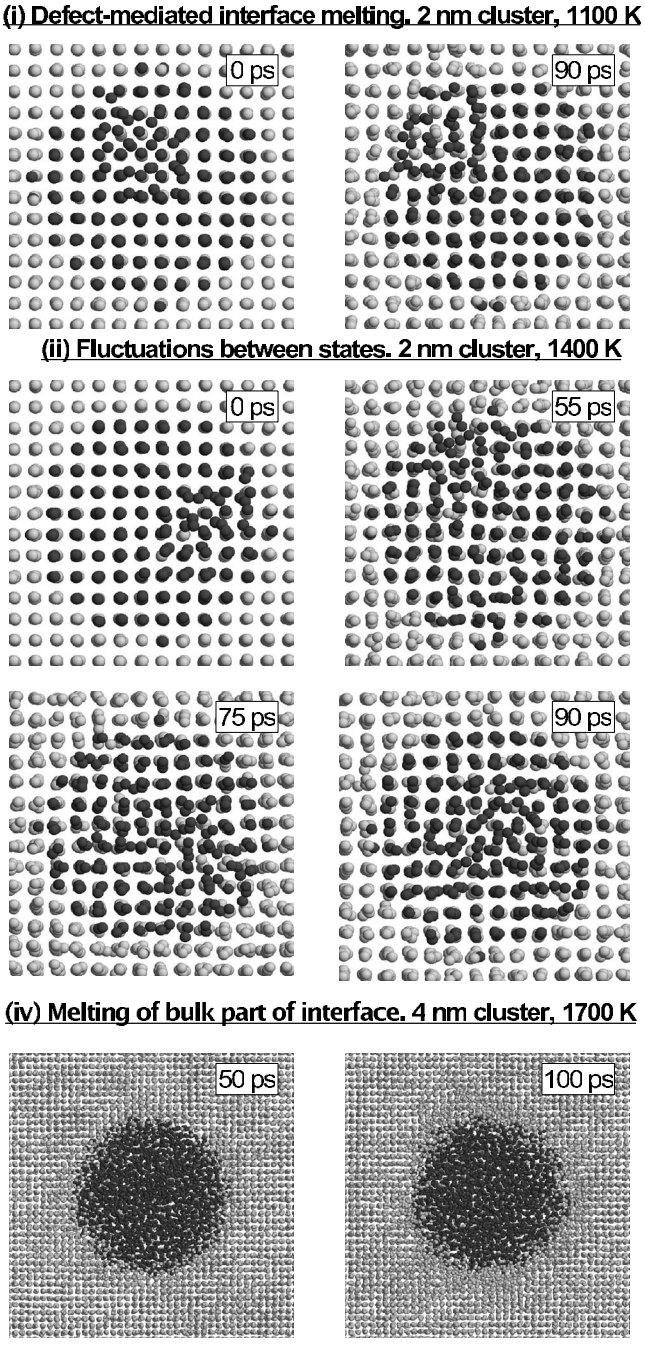

FIG. 3. Illustration of the melting mechanisms of Cu nanocrystals in Co. The atom positions are *not* time averaged. Darker spheres illustrate Cu atoms and lighter ones illustrate Co. The figures are cross sections of the middle of the simulation cells. The simulations were started at a temperature of 100 K in all cases, and the cells were heated up in all cases to within 30 K of the final temperature in 50 ps.

plot in Fig. 4, where symbols are used to show the state of the system for each temperature-size combination.

C. Angular structure factor analysis

To quantitatively analyze the melting mechanisms, we carried out angular structure factor analysis[44,45] of the nano-

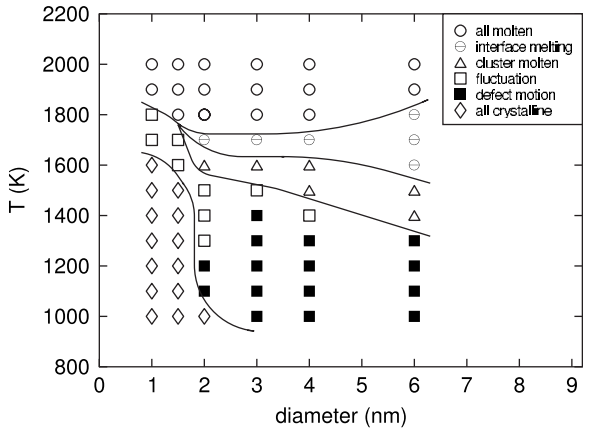

FIG. 4. Phase-diagram-like plot of the different observed states of Cu nanocrystals embedded in a Co matrix. The lines are guides for the eyes to allow for easy distinction of the different regions. For detailed descriptions of the mechanisms, see text.

crystal and matrix atoms. This approach uses the angles between bonds to nearest neighbors to calculate a structure factor $P_{\mathrm{st}}(i)$ for each atom i. This value is normalized in such a way that the angular structure factor of an atom in a perfect lattice is exactly 0, and in a perfect lattice position with thermal displacements it is close to zero. In an amorphous or liquid surrounding the structure factor of an atom is around 0.5. This approach has also previously been shown to correspond well to a kinetic-energy criterion for detecting local transient molten zones.[46]

For the purposes of the current paper the absolute scale of the P_{st} values are not important. Instead it is sufficient to note that high values of P_{st} correspond to a higher degree of disorder, i.e., melting. To analyze the degree of melting, we calculated the $P_{\mathrm{st}}(i)$ separately for nanocrystal and matrix atoms in several melting runs. In accordance with Ref. 45, atoms with a structure factor higher than 0.2 were considered to be disordered (defect or liquidlike atoms). To reduce short-time scale fluctuations, the results were further time averaged over 5 ps time intervals.

Since the embedded nanocrystals always have a partly disordered interface with the surroundings and the simulation cell is finite, the average structure factor for the nanocrystal $\langle P_{\mathrm{st}}^{\mathrm{cr}} \rangle$ as well as the matrix $\langle P_{\mathrm{st}}^{\mathrm{ma}} \rangle$ will be nonzero also at the beginning of the simulations. If a nanocrystal melts partly or fully during a simulation starting from a low temperature, $\langle P_{\mathrm{st}}^{\mathrm{cr}} \rangle$ will increase with time due to the increased disorder. Moreover, if the surrounding matrix melts partly or fully, $\langle P_{\mathrm{st}}^{\mathrm{ma}} \rangle$ will also increase.

Results from the P_{st} analysis are shown for 2 nm clusters in Figs. 5 and 6. The figures show the fraction f_{dis} of cluster or matrix atoms that are disordered ($P_{\mathrm{st}} > 0.2$). If a nanocrystal melts partly or fully during a simulation starting from a low temperature, $f_{\mathrm{dis}}^{\mathrm{cluster}}$ will increase with time due to the increased disorder. Moreover, if the surrounding matrix melts partly or fully, $f_{\mathrm{dis}}^{\mathrm{matrix}}$ will also increase. The results of f_{dis} can be compared with the mechanisms indicated in Fig. 4 for a cluster diameter of 2 nm.

Inspection of Fig. 5 shows that in all cases the degree of disorder in the Cu nanocrystal first drops. This is because the

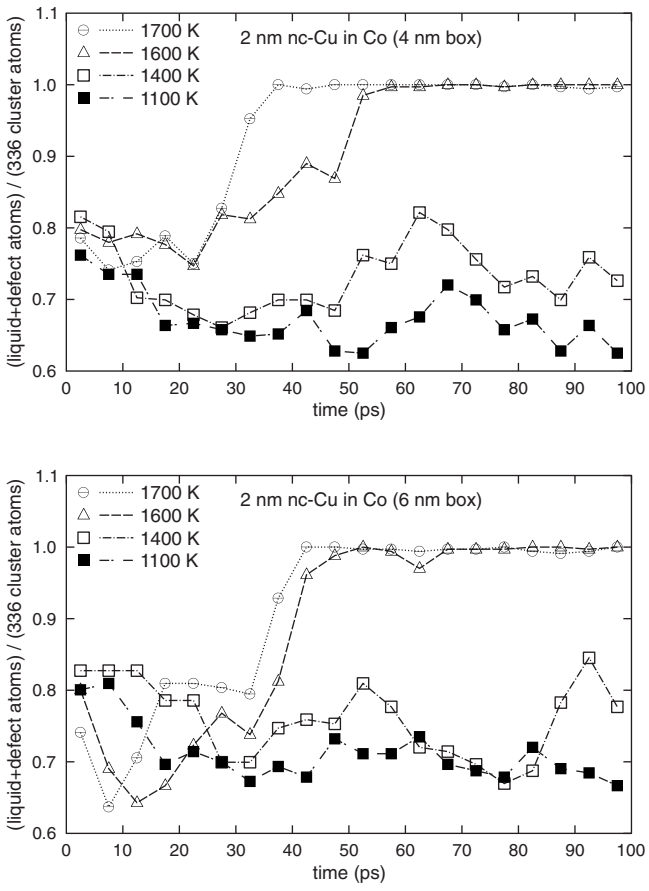

FIG. 5. Results for angular structure factor analysis of 2 nm Cu nanocrystals in Co—fraction of atoms with a structure factor associated with defective or liquid atoms (cf. Ref. 45). (a) shows results for a nanocrystal in a 4 nm side length simulation cell. (b) shows results for a 6 nm side length simulation cell. The simulations were started at a temperature of 100 K in all cases, and the cells were heated up in all cases to within 30 K of the final temperature in 50 ps.

simulation is started at 100 K, and while the cluster is heated up during the first 50 ps, the interface first reorganizes into a more ordered state. For the determination of the melting mechanisms, the most interesting is the behavior after about 20 ps.

At the lowest temperature, 1100 K, the degree of disorder continues dropping and reaches a roughly constant value. This is consistent with the behavior expected for mechanism (i) described in text—partial interface melting. At 1400 K the degree of disorder is slightly higher and varies more with time, as expected for mechanism (ii)—fluctuations between states. At 1600 and 1700 K the cluster melts completely ($f_{\mathrm{dis}}^{\mathrm{cluster}} = 1.0$), as expected for mechanisms (iii) and (iv).

Figure 6 shows the degree of disorder of the matrix atoms $f_{\mathrm{dis}}^{\mathrm{matrix}}$ in the same simulations. The initial value of 0.29 is relatively high because strained atoms close to the interface become counted as disordered ones by the limit used, but as discussed above the absolute value is not significant in the current context. After the final temperature has been reached at 50 ps, $f_{\mathrm{dis}}^{\mathrm{matrix}}$ remains practically unchanged at 1100 and 1400 K. This is as expected from the description of mecha-

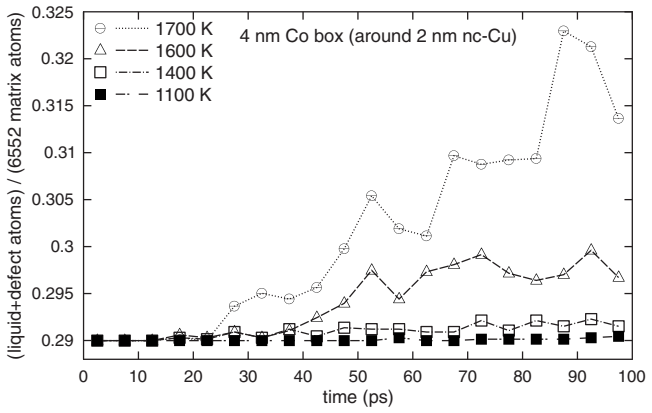

FIG. 6. Results for angular structure factor analysis of the Co matrix surrounding a 2 nm Cu nanocrystal—fraction of atoms with a structure factor associated with defective or liquid atoms (cf. Ref. 45). The simulations were started at a temperature of 100 K in all cases, and the cells were heated up in all cases to within 30 K of the final temperature in 50 ps.

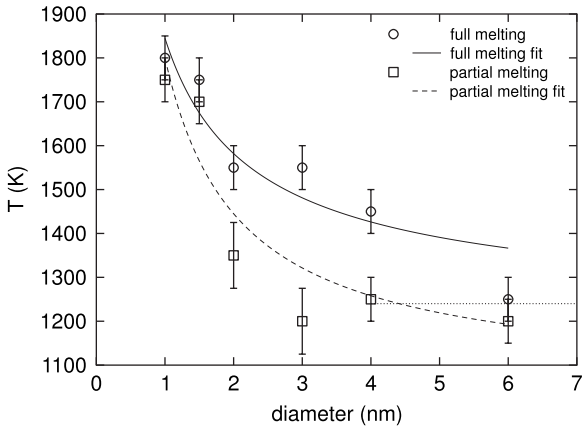

FIG. 7. Dependence of the partial and full melting temperatures of the Cu nanoclusters on the diameter. The lines are fits of a curve of the form 1 per diameter to the data. The horizontal line shows the melting points of Cu in the bulk phase within the potential model used.

nisms (i) and (ii); since only the nanocluster partly melts, no change in the matrix disorder is expected. At 1600 K $f_{\mathrm{dis}}^{\mathrm{matrix}}$ somewhat increases as the cluster fully melts [mechanism (iii)] and increases the disorder at the interface. At 1700 K $f_{\mathrm{dis}}^{\mathrm{matrix}}$ strongly increases and fluctuates because the matrix melts close to the nanocrystal interface, as expected for mechanism (iv). Note, however, that the degree is disorder still remains much below 1.0, confirming that the whole matrix does not melt.

Thus we conclude that the quantitative structure factor analysis gives results which are fully consistent with the description of melting mechanisms (i)–(iv) given in Sec. III B based on visual analysis.

The results for the Cu cluster are also shown for two different simulation cell sizes, see Figs. 5(a) and 5(b). The behavior is, excepted for different random thermal fluctuations, exactly the same for the two box sizes, confirming that the results are not dependent on the box size. Also simulations for some other cluster sizes were repeated with a larger box size (cube length three times the cluster diameter rather than two times), and in all cases the melting mechanism was not dependent on the simulation cell sizes.

D. Other systems

Similar premelting behavior as that in the Cu in Co system was also observed in the Ag in Cu and Au in Cu systems. However, since the melting temperature difference between the two elements is small, it was difficult to give quantitative temperature limits for the various states. Hence these systems were not analyzed in as great detail as the Cu in Co one.

The Si in silica system also showed a similar region of premelting, which is well visible in Fig. 1. Visual analysis of the system in this temperature regime showed that at the lower temperatures, groups of about 5–20 atoms were formed where the atoms exchanged positions with each other. This behavior is similar to the onset of interstitial-mediated melting previously described for bulk Cu (Refs. 47 and 48) and can be considered a form of fluctuations of the state of the cluster [mechanism (i) if it occurs only at the interface and mechanism (ii) if it occurs everywhere in the cluster]. At higher temperatures the cluster melted at the interface prior to its full melting.

IV. DISCUSSION

The dependence of $T_{\mathrm{melt,partial}}$ and $T_{\mathrm{melt,cluster}}$ on the cluster diameter d for the Cu in Co system is illustrated in Fig. 7. The data were, considering the uncertainty of ± 50 K from the temperature interval of 100 K, well fit by functions of the form $T_0 + a/d$, where d is the diameter of the cluster and a and T_0 are fitted constants. Fitting a modified functional form of $T_0 + a/d^b$ gave values of b very close to 1, showing that the functional form indeed is of the form $1/d$.

The observed $1/d$ behavior is well in line with several analytical models of the melting of nanocrystals.[10,12,17,22,49,50] However, in most previous cases studying nanocrystals in vacuum, the direction has been the opposite since those clusters melt completely below the bulk melting point, whereas our embedded clusters fully melt above it (see Fig. 1). These models are based on considerations of how the surface and interface energies affect the cohesion and melting of the crystals. On the other hand, it is clear that a single analytical model clearly cannot describe all aspects of the complex melting mechanisms illustrated in Fig. 4.

The observation that defects can migrate in the nanocluster [mechanism (i)] resembles experimental observations for Xe bubbles in Al, where motion of dislocation was directly observed.[51] However, in the case of dislocations no association was made with melting. The migration we observe occurs on more than 10 orders of magnitude faster time scales than the dislocation motion and would thus in experimental observation be visible as a random change in the nanocrystal atom positions which could be easily confused with complete melting. The observation that the first stage of melting

is defect migration to the interface is also well in line with experimental observations that the melting of In particles in Al starts from the side facets of the particle.[4,52]

The fluctuations between different states of the system at the same temperature [mechanism (ii)] are similar to the fluctuations previously reported for nanoclusters in vacuum.[1,53] Mechanism (iv), melting of the bulk part of the interface, can be understood in terms of interface melting. Several theoretical models of surface and interface melting have been presented,[43,54,55] and very recently a Landau model of melting has been extended to describe the melting of surface layers of nanoparticles.[50] Although these models focus on the melting of the nanoparticle, many of the models show that in an interfacial system the disorder can extend also to the other side of the interface.[43] A somewhat similar effect to mechanisms (iv) was also reported by Jin *et al.*,[26] who showed that a small core can induce the melting of a larger surrounding nanoparticle.

Our overall result that the melting point of embedded nanocrystals is not well defined but that a regime of different melting mechanisms exists shows that the common assumption in nanocrystal melting models of a single melting point is not well justified.[10,18] However, our observations are in excellent agreement with very recent experimental result[15] which show that the melting of Cu nanocrystals involve at least two stages and a report that the melting of Au nanocrystals occurs gradually.[9]

Our results in fact suggest a likely explanation to the large differences in reported melting temperatures of embedded nanocrystals. Note that melting begins below the bulk melting temperature but is not complete until well above it (see Fig. 1). Different experimental methods may give different interpretations of the different stages. The first mechanisms (i) and (ii) of defect motion and fluctuation occur when the nanocrystal still clearly remains overall crystalline. However, the migration and fluctuations occur on subnanosecond timescales, so if the clusters are imaged in real space on macroscopic timescales, they could appear molten as the experimental image would average over very large numbers of atom positions changed by the atom motion. For mechanism (i) the experimental image could seem like interface melting, and for mechanism (ii) it could seem like full melting of the cluster. This could specifically be the case in transmission-electron microscopy (real-space images)[4,52] and Rutherford backscattering/channeling experiment.[8,11,14,54] On the other hand, methods which measure the average atomic short-range order such as Raman and certain x-ray approaches[14,56] would be expected to interpret nanocrystals to still remain crystalline during the defect motion state.

The current results also have bearing on several potential application areas of nanocrystals. The different stages of nanocrystal melting need to be considered when interpreting results of laser processing of nanocrystals, where strong heating of the crystals has been used to control the strain state of the system.[3] The observation that atom reorganization can begin in nanocrystals well below their melting temperature needs to be considered when planning annealing temperature ranges for nanocrystals. The atom reorganization might in fact aid the crystallization of the nanocrystals at the end of an Ostwald ripening[57,58] annealing. On the other hand, if the defects freeze in after the annealing, they are likely to affect the electrical and optical properties of the crystals.[59]

V. CONCLUSIONS

In conclusion, we have shown that nanocrystals embedded in a solid bulk with a higher melting temperature exhibit a many-faceted melting behavior. We observe four different mechanisms that precede full melting of the system. These are, in order of increasing temperature, (i) defect motion in the cluster leading to partial interface melting, (ii) fluctuations between ordered and disordered states, (iii) melting of the nanocrystal but not the surrounding bulk, and (iv) melting of the surrounding bulk at the interface with the nanocrystal. While all of the mechanisms have in some form been previously reported in the literature, the current work showed that even a single system can have at least four different stages of melting. We further argue that due to this complexity, different experimental methods may interpret the same system as either molten or crystalline due to the different ways the atomic state is measured.

ACKNOWLEDGMENTS

We thank K. Albe and T. T. Järvi for useful discussions. This work was performed within the Finnish Centre of Excellence in Computational Molecular Science (CMS), financed by The Academy of Finland and the University of Helsinki, and also financed by Academy projects OPNA and CONADEP. Grants of computer time from the Center for Scientific Computing in Espoo, Finland, are gratefully acknowledged.

*kai.nordlund@helsinki.fi

[1] F. Baletto and R. Ferrando, Rev. Mod. Phys. **77**, 371 (2005).
[2] B. Jalali, Sci. Am. **296**, 46 (2007).
[3] L. Khriachtchev, M. Räsänen, and S. Novikov, Appl. Phys. Lett. **88**, 013102 (2006).
[4] Q. S. Mei and K. Lu, Prog. Mater. Sci. **52**, 1175 (2007).
[5] G. A. Breaux, R. C. Benirschke, T. Sugai, B. S. Kinnear, and M. F. Jarrold, Phys. Rev. Lett. **91**, 215508 (2003).
[6] J. Akola and M. Manninen, Phys. Rev. B **63**, 193410 (2001).
[7] A. vom Felde, J. Fink, Th. Muller-Heinzerling, J. Pflüger, B. Scheerer, G. Linker, and D. Kaletta, Phys. Rev. Lett. **53**, 922 (1984).
[8] K. K. Bourdelle, A. Johansen, and E. Johnson, Nucl. Instrum. Methods Phys. Res. B **118**, 478 (1996).
[9] D. Dalacu and L. Martinu, Appl. Phys. Lett. **77**, 4283 (2000).
[10] G. Kellermann and A. F. Craievich, Phys. Rev. B **65**, 134204 (2002).
[11] H. Rösner, P. Scheer, J. Weissmüller, and G. Wilde, Philos. Mag.

Lett. **83**, 511 (2003).
[12] A. Singh and A. P. Tsai, Sadhana: Proc., Indian Acad. Sci. **28**, 63 (2003).
[13] H. Rösner and G. Wilde, Scr. Mater. **55**, 119 (2006).
[14] I. D. Sharp, Q. Xu, and D. O. Yi, J. Appl. Phys. **100**, 114317 (2006).
[15] O. A. Yeshchenko, I. M. Dmitruk, A. A. Alexeenko, and A. M. Dmytruk, Phys. Rev. B **75**, 085434 (2007).
[16] N. Boucharat, H. Rösner, and G. Wilde, Mater. Sci. Eng., A **449-451**, 640 (2007).
[17] Q. Jiang, Z. Zhangd, D. T. Tsu, H. Y. Tong, and M. Iskandar, J. Mater. Sci. **34**, 5919 (1999).
[18] L. F. Cao, G. Y. Xu, D. Xie, M. X. Guo, L. Luo, Z. Li, and M. P. Wang, Phys. Status Solidi B **243**, 2745 (2006).
[19] D. Xie, M. P. Wang, W. H. Qi, and L. F. Cao, Mater. Chem. Phys. **96**, 418 (2006).
[20] Q. Xu *et al.*, Phys. Rev. Lett. **97**, 155701 (2006).
[21] K. Lu and Z. H. Jin, Curr. Opin. Solid State Mater. Sci. **5**, 39 (2001).
[22] S. Valkealahti and M. Manninen, Z. Phys. D: At., Mol. Clusters **26**, 255 (1993).
[23] A. Rytkönen, H. Häkkinen, and M. Manninen, Eur. Phys. J. D **9**, 451 (1999).
[24] S. Kummel, J. Akola, and M. Manninen, Phys. Rev. Lett. **84**, 3827 (2000).
[25] E. Kesala, A. Kuronen, and K. Nordlund, Phys. Rev. B **75**, 174121 (2007).
[26] Z. H. Jin, H. W. Sheng, and K. Lu, Phys. Rev. B **60**, 141 (1999).
[27] M. O. Pedersen, I. A. Bönicke, E. Lægsgaard, I. Stensgaard, A. Ruban, J. K. Norskov, and F. Besenbacher, Surf. Sci. **387**, 86 (1997).
[28] C. G. Zimmermann, K. Nordlund, M. Yeadon, J. M. Gibson, R. S. Averback, U. Herr, and K. Samwer, Phys. Rev. B **64**, 085419 (2001).
[29] M. S. Daw, S. M. Foiles, and M. I. Baskes, Mater. Sci. Rep. **9**, 251 (1993).
[30] L. Pavesi, L. D. Negro, C. Mazzoleni, G. Franzò, and F. Priolo, Nature (London) **408**, 440 (2000).
[31] L. Khriachtchev, M. Räsänen, S. Novikov, and J. Sinkkonen, Appl. Phys. Lett. **79**, 1249 (2001).
[32] J. Frantz and K. Nordlund, Phys. Rev. B **67**, 075415 (2003).
[33] T. T. Jarvi, A. Kuronen, K. Meinander, K. Nordlund, and K. Albe, Phys. Rev. B **75**, 115422 (2007).
[34] K. Meinander, T. T. Järvi, and K. Nordlund, Appl. Phys. Lett. **89**, 253109 (2006).
[35] K. Nordlund and R. S. Averback, Phys. Rev. B **59**, 20 (1999).
[36] S. M. Foiles, M. I. Baskes, and M. S. Daw, Phys. Rev. B **33**, 7983 (1986); **37**, 10378 (1988).
[37] T. Watanabe, D. Yamasaki, K. Tatsumura, and I. Ohdomari, Appl. Surf. Sci. **234**, 207 (2004).
[38] J. Samela, K. Nordlund, V. N. Popok, and E. E. B. Campbell, Phys. Rev. B **77**, 075309 (2008); this also has the description of the Samela-Watanabe potential.
[39] S. von Alfthan, A. Kuronen, and K. Kaski, Phys. Rev. B **68**, 073203 (2003).
[40] F. Djurabekova, M. Backman, and K. Nordlund, Nucl. Instrum. Methods Phys. Res. B **266**, 2683 (2008).
[41] H. J. C. Berendsen, J. P. M. Postma, W. F. van Gunsteren, A. DiNola, and J. R. Haak, J. Chem. Phys. **81**, 3684 (1984).
[42] See EPAPS Document No. E-PRBMDO-79-079904 for supplementary information and more examples. For more information on EPAPS, see http://www.aip.org/pubservs/epaps.html or ftp.aip.org in the directory epaps/.
[43] R. Lipowsky, Phys. Rev. Lett. **49**, 1575 (1982).
[44] H. Zhu, R. S. Averback, and M. Nastasi, Philos. Mag. A **71**, 735 (1995).
[45] K. Nordlund and R. S. Averback, Phys. Rev. B **56**, 2421 (1997).
[46] K. Nordlund, M. Ghaly, R. S. Averback, M. Caturla, T. Diaz de la Rubia, and J. Tarus, Phys. Rev. B **57**, 7556 (1998).
[47] K. Nordlund and R. S. Averback, Phys. Rev. Lett. **80**, 4201 (1998).
[48] M. Forsblom and G. Grimvall, Nature Mater. **4**, 388 (2005).
[49] L. J. Lewis, P. Jensen, and J.-L. Barrat, Phys. Rev. B **56**, 2248 (1997).
[50] A. P. Chernyshev, Mater. Chem. Phys. **112**, 226 (2008).
[51] R. C. Birtcher, S. E. Donnelly, M. Song, F. Furuya, K. Mitsuishi, and C. W. Allen, Phys. Rev. Lett. **83**, 1617 (1999).
[52] K. Sasaki and H. Saka, Philos. Mag. A **63**, 1207 (1991).
[53] D. Schebarchov and S. C. Hendy, Phys. Rev. Lett. **96**, 256101 (2006).
[54] J. W. M. Frenken and J. F. van der Veen, Phys. Rev. Lett. **54**, 134 (1985).
[55] J. G. Dash, A. W. Rempel, and J. S. Wettlaufer, Rev. Mod. Phys. **78**, 695 (2006).
[56] B. Johannessen, P. Kluth, D. J. Llewellyn, G. J. Foran, D. J. Cookson, and M. C. Ridgway, Appl. Phys. Lett. **90**, 073119 (2007).
[57] W. Ostwald, Z. Elektrochem. Angew. Phys. Chem. **22**, 289 (1897).
[58] K. H. Heinig, B. Schmidt, A. Markwitz, R. Grötzchel, M. Strobel, and S. Oswald, Nucl. Instrum. Methods Phys. Res. B **148**, 969 (1999).
[59] R. Salh, L. Fitting, E. V. Kolesnikova, A. A. Sitnikova, M. V. Zamoryanskaya, B. Schmidt, and H. J. Fitting, Semiconductors **41**, 381 (2007).